Molecular Cell, Vol. 8, 351–361, August, 2001, Copyright ©2001 by Cell Press

Structure of the TRFH Dimerization Domain of the Human Telomeric Proteins TRF1 and TRF2

Louise Fairall,[1,4] Lynda Chapman,[1,4] Heidi Moss,[2] Titia de Lange,[2] and Daniela Rhodes[1,3]
[1]MRC Laboratory of Molecular Biology
Hills Road
Cambridge CB2 2QH
United Kingdom
[2]The Rockefeller University
New York, New York 10021

Summary

TRF1 and TRF2 are key components of vertebrate telomeres. They bind to double-stranded telomeric DNA as homodimers. Dimerization involves the TRF homology (TRFH) domain, which also mediates interactions with other telomeric proteins. The crystal structures of the dimerization domains from human TRF1 and TRF2 were determined at 2.9 and 2.2 Å resolution, respectively. Despite a modest sequence identity, the two TRFH domains have the same entirely α-helical architecture, resembling a twisted horseshoe. The dimerization interfaces feature unique interactions that prevent heterodimerization. Mutational analysis of TRF1 corroborates the structural data and underscores the importance of the TRFH domain in dimerization, DNA binding, and telomere localization. A possible structural homology between the TRFH domain of fission yeast telomeric protein Taz1 with those of the vertebrate TRFs is suggested.

Introduction

Telomeres are protein-DNA complexes that protect chromosome ends from being recognized and processed as DNA breaks (Lundblad, 2000). Mammalian telomeres contain long tandem arrays of double-stranded TTAGGG repeats that are maintained by the telomerase and act as binding sites for two related DNA binding proteins, TRF1 (Chong et al., 1995) and TRF2 (Broccoli et al., 1997). TRF1 acts as a negative regulator of telomere maintenance. Overexpression of TRF1 results in telomere shortening, and a dominant negative allele of TRF1 induces inappropriate telomere elongation (Smogorzewska et al., 2000; van Steensel and de Lange, 1997). Like the budding yeast telomeric protein, scRap1p (Marcand et al., 1997a), TRF1 is thought to act in *cis* to control telomere extension at individual chromosome ends. TRF1 binds to the telomeric proteins tankyrase and TIN2, which also contribute to telomere length regulation (Smith et al., 1998; Kim et al., 1999; Smith and de Lange, 2000). Similarly, TRF2 and its binding partner hRap1, the human ortholog of scRap1p, affect telomere length maintenance in human cells (Li et al., 2000; Smogorzewska et al., 2000). Furthermore, TRF2 plays a key role in the protection of chromosome ends. Expression of a dominant negative allele of TRF2 results in immediate destabilization of mammalian chromosomes and rapid induction of cell cycle arrest and apoptosis (Karlseder et al., 1999; van Steensel et al., 1998). In general, mammalian cells respond to TRF2 deficiency as if their natural chromosome ends resemble DNA breaks, resulting in degradation of the single-stranded telomeric overhang, inappropriate ligation of chromosome ends, and activation of the ATM/p53 DNA damage response pathway (Karlseder et al., 1999; van Steensel et al., 1998).

Similarly, fission yeast telomeres are protected from end-to-end fusions and recombination by a TRF-related protein, Taz1, that binds to duplex telomeric DNA (Ferreira and Cooper, 2001; Nakamura et al., 1998). Like TRF1 and TRF2, Taz1 acts as a negative regulator of telomere length (Cooper et al., 1997; Nimmo et al., 1998). Remarkably, budding yeast lacks a TRF-like telomeric protein, and in this organism scRap1p is the main factor that binds duplex telomeric DNA and regulates telomere length (Marcand et al., 1997a; 1997b; McEachern et al., 2000).

The TRF family of proteins have similar architectures, defined by two sequence features (Figure 1A). First, these proteins have C-terminal DNA binding motifs that are closely related to the Myb domain of c-Myb (Nishikawa et al., 1998; Ogata et al., 1994) and also to the Myb/homeodomains of the budding yeast Rap1p (Konig et al., 1996; Konig and Rhodes, 1997). Second, these proteins have a centrally located sequence motif of about 200 aa, referred to as the TRF homology (TRFH) domain that is unique to this gene family (Broccoli et al., 1996, 1997; Li et al., 2000). The TRFH domains are more divergent in sequence than are their adjacent Myb motifs (Figure 1A) and overlap with a protein-protein interaction domain that mediates strong homotypic interactions (Bianchi et al., 1997; Broccoli et al., 1997).

TRF1 is a homodimer in vivo, and its accumulation at telomeres depends on homotypic interactions (Bianchi et al., 1997; van Steensel and de Lange, 1997). Similarly, the TRF2 TRFH domain mediates homotypic interactions (Broccoli et al., 1997), but TRF1 and TRF2 do not form heterodimers (Broccoli et al., 1997; Zhu et al., 2000). The TRFH domain of Taz1 may also be responsible for homotypic interactions because Taz1, like TRF1 and TRF2, binds telomeric DNA as a dimer (Spink et al., 2000). Besides their function in dimerization, the TRFH domains of the vertebrate TRFs are involved in the recruitment of interacting partners to the telomeres. TIN2 interacts the TRFH domain of TRF1 (Kim et al., 1999; L.C. and D.R., unpublished data), whereas the TRFH domain of TRF2 is involved in the binding of hRap1 (Li et al., 2000).

The juxtaposition of two Myb DNA binding domains appears to be a characteristic of all duplex telomeric DNA binding proteins identified to date. Whereas the budding yeast Rap1p has two tandemly arranged Myb/homeodomains within a monomeric protein (Konig et al., 1996), the mammalian TRFs and the fission yeast Taz1 achieve this by using the alternative strategy of

[3]Correspondence: rhodes@mrc-lmb.cam.ac.uk
[4]These authors contributed equally to this work.

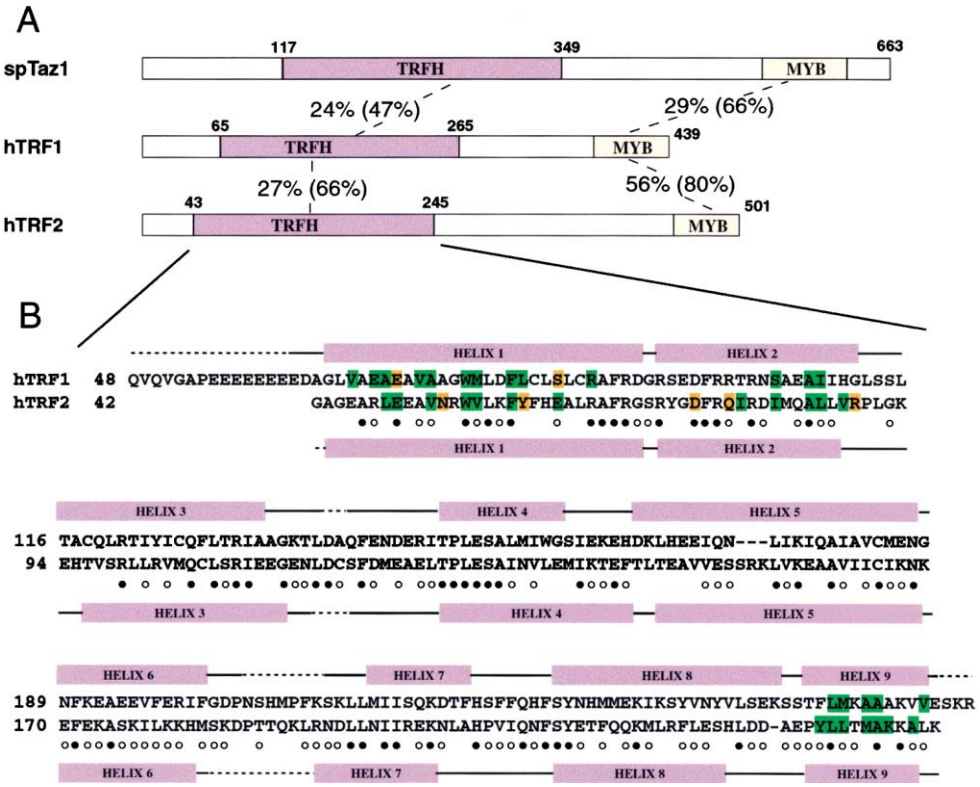

Figure 1. Architecture of the TRF Family of Telomeric Proteins and Secondary Structure of the TRFH Domain from Human TRF1 and TRF2

(A) Overview of the shared domain structure of human TRF1 and TRF2 and the fission yeast Taz1. TRFH indicates the TRF homology domain and Myb the DNA binding domain, and their percentage sequence identity and (similarity) are shown.

(B) Secondary structure elements in the dimerization domains of TRF1 and TRF2. Identical residues are indicated by black dots and similar residues by circles. The positions of the α helices are indicated by solid-lilac rectangles, and broken lines indicate regions of structural disorder. Amino acids side chains involved in forming the dimer interface are indicated: residues involved in hydrophobic interactions are shown in green, and those involved in hydrogen bonds are shown in orange.

dimerization (Bianchi et al., 1997; Broccoli et al., 1997; Spink et al., 2000; van Steensel and de Lange, 1997). An optimal telomeric binding site for a TRF1 homodimer contains two YTAGGGTTR halfsites, each bound by one Myb domain (Bianchi et al., 1999; Konig et al., 1998). Interestingly, the relative orientation and spacing of the two halfsites does not affect the DNA binding affinity of TRF1, suggesting that TRF1 has an unusual structure in which the Myb DNA binding domain is connected to the TRFH domain by a long, highly flexible linker (Bianchi et al., 1999). TRF2, which has a similar domain structure, can also bind to YTAGGGTTR halfsites with variable spacing and orientation (A. Bianchi, M. van Breugel, R. Wang, and T.d.L., unpublished data), consistent with a similarly versatile DNA binding mode.

The flexible DNA binding mode of TRF1 and TRF2 is likely to be relevant to the unusual overall architecture of telomeric chromatin. Telomeres of mammals, ciliates, and trypanosomes can adopt a lasso-like structure, called the t-loop, in which the telomere terminus is folded back and the single-stranded overhang invades the duplex telomeric DNA (Griffith et al., 1999; Munoz-Jordan et al., 2001; Murti and Prescott, 1999). T-loops have been proposed to prevent the chromosome end from being recognized as damaged DNA and could contribute to the regulation of the telomerase activity (Griffith et al., 1999). Although it is not known how t-loops are formed in vivo, TRF2 has the ability to remodel a telomere model substrate into a looped configuration (Griffith et al., 1999), and TRF1 can loop and pair telomeric DNA (Bianchi et al., 1999; Griffith et al., 1998). It is likely that the ability of TRF1 and TRF2 to change the shape of telomeric DNA is a reflection of their oligomeric nature, as well as their structural flexibility, allowing apposition of two distant telomeric sites by the tethering of two Myb domains in one DNA binding unit. Thus, the homodimerization, as mediated by the TRFH domain, is likely to be a crucial aspect of the function of these proteins.

Here, we present the 3D structure of the dimerization domain from both human TRF1 and TRF2. Despite a modest sequence conservation, the two domains have the same entirely α-helical architecture, and dimerization occurs via three α helices from each monomer. These structures explain why TRF1 and TRF2 form only homodimers and not heterodimers. The structural interpretation is corroborated by biochemical and genetic data that confirm the importance of the interface in dimerization, DNA binding, and telomere localization. Secondary structure predictions suggest that the TRFH domain of fission yeast Taz1 also has an entirely α-helical fold that might be related to that of the vertebrate TRFs.

Table 1. Summary of Crystallographic Analysis

	hTRF1					hTRF2		
Crystal	Native 1	Native 2	EMTS	PtCl4	Xenon	Native	EMTS	Se-Met
Resolution (wavelength) (Å)	3.0 (0.92)	2.9 (0.87)	3.0 (0.87)	3.0 (0.87)	3.0 (1.54)	2.2 (0.87)	2.7 (1.54)	2.5 (0.95)
Reflections, observed/unique	85,431/8,046	45,019/8,514	57,542/8,231	54,534/8,062	44,608/8,133	89,685/24,415	26,200/12,565	58,951/16,438
Rsym (completeness) (%)	5.9 (99.7)	5.7 (97.1)	8.1 (99.8)	6.6 (99.8)	5.6 (99.9)	5.2 (99.1)	7.3 (95.5)	7.0 (99.2)
	MIR Analysis Using Native 1					MIR Analysis		
Mean fractional isomorphous difference (%)			20.9	16.1	7.0		18.0	14.7
Phasing power isomorphous/anomalous[b]			0.67/0.71	0.36/0.24	1.25/0.67		0.98/0.75	1.45/1.26
Cullis R-factor isomorphous/anomalous			0.88/0.89	0.97/0.99	0.77/0.97		0.85/0.66	0.79/0.83
Mean overall figure of merit centric/acentric	0.34/0.43					0.301/0.246		
	Refinement Using Native 2					Refinement		
Resolution (Å)		24.84 − 2.9				23.72 − 2.2		
R factor/free R-factor (%)[c]		25/30.3				23.5/26.8		
Reflections, $\|F\| > 2.0\ \|F\|$ working/test		7385/801				21,482/2,285		
Molecules/asymmetric unit		1 monomer				2 monomers		
Total no. of atoms		1475				2923		
No. of water molecules		None				136		
No. of magnesium atoms		None				1		
Rms deviations bond lengths (Å)		0.008				0.006		
Rms deviations bond angles (degrees)		1.4				1.1		
Ramachandran favored/allowed/generously allowed %		82.2/16.1/1.7				91.0/8.1/0.9		

[a] Rsym = $\Sigma|I - \langle I\rangle|/\Sigma\langle I\rangle$, where I and $\langle I\rangle$ are the measured and averaged intensities of multiple measurements of the same reflection.
[b] Phasing power = rms. ($\langle F_H\rangle/E$), where F_H is the calculated structure factor of the heavy atoms, and E is the residual lack of closure.
[c] R factor = $\Sigma||Fo| - Fc||/\Sigma|Fo|$, where Fo is the observed structure factor amplitude, and Fc is the structure factor calculated from the model.

Results and Discussion

Crystal Structure Determination

Proteolysis studies (not shown) and DNA binding studies (Bianchi et al., 1999) revealed that both TRF1 and TRF2 consist of flexibly linked functional and structural domains, explaining the failure to crystallize the full-length proteins. Therefore, we focused on the conserved TRFH domain from both proteins (Broccoli et al., 1997). Constructs for expression in *E. coli* were based on previous deletion analysis of the dimerization domain of TRF1 (Bianchi et al., 1997), on sequence comparison of the mouse and human TRFs, and on the location of the proteolysis sites that defined a protease resistant domain that encompasses the TRFH domain of both TRF1 and TRF2. The recombinant purified proteins (residues 48–268 of human TRF1 and residues 42–245 of human TRF2) used in the crystallographic analysis form homodimers in solution, as judged from gel filtration analysis (not shown), and hence contain the dimerization domain of the TRFs. Both dimerization domains contain additional residues N and C terminally to the region defined as the TRFH domain from sequence alignments (Li et al., 2000). The crystal structures of the two dimerization domains were determined independently by multiple isomorphous replacement methods (Table 1). The model of the TRF1 dimerization domain contains residues 62–265, and that of TRF2 contains residues 43–245 with short stretches of the same two internal loops missing in the electron density maps, presumably due to flexibility in these regions of the two structures. Residues at the N and C termini of both proteins are also not visible (Figure 1B). The structure of the dimerization domain of TRF1 was solved to 2.9 Å resolution and that of TRF2 to 2.2 Å resolution (Table 1). Representative regions of the experimental electron density maps are shown in Figure 4.

The Dimerization Domains of TRF1 and TRF2 Have the Same Architecture

The superposition of the structure of the dimerization domain of TRF1 with that of TRF2 shows that despite a modest sequence conservation over this region (27% identity), the two domains have almost identical 3D structures (Figure 2A). Each dimer is formed by two monomers interacting in an antiparallel arrangement forming a symmetrical dimer whose overall structure resembles a twisted horseshoe.

The structure of the TRF1 and TRF2 monomers consists of nine α helices, forming an elongated helix bundle (Figure 2B). The four monomers in the two dimers (helices 1–6 and 9) superimpose with a root-mean-square deviation (rmsd) between Cα atoms of 1.23 Å and hence are structurally very similar. The topology can be viewed as consisting of three pairs of α helices (1 and 2, 4 and 5, 6 and 7) packing against helices 3 and 8 (Figure 2B). Coming out of helix 7, the loop and helix 8 run across the surface of the helix bundle, forming a strut that stabilizes the structure. Helix 9 packs almost perpendicularly on helix 1, explaining the large size of the dimerization domain of the TRFs (Figure 2B).

Although the number of α helices and their position in the amino acid sequences of the TRFH domains of

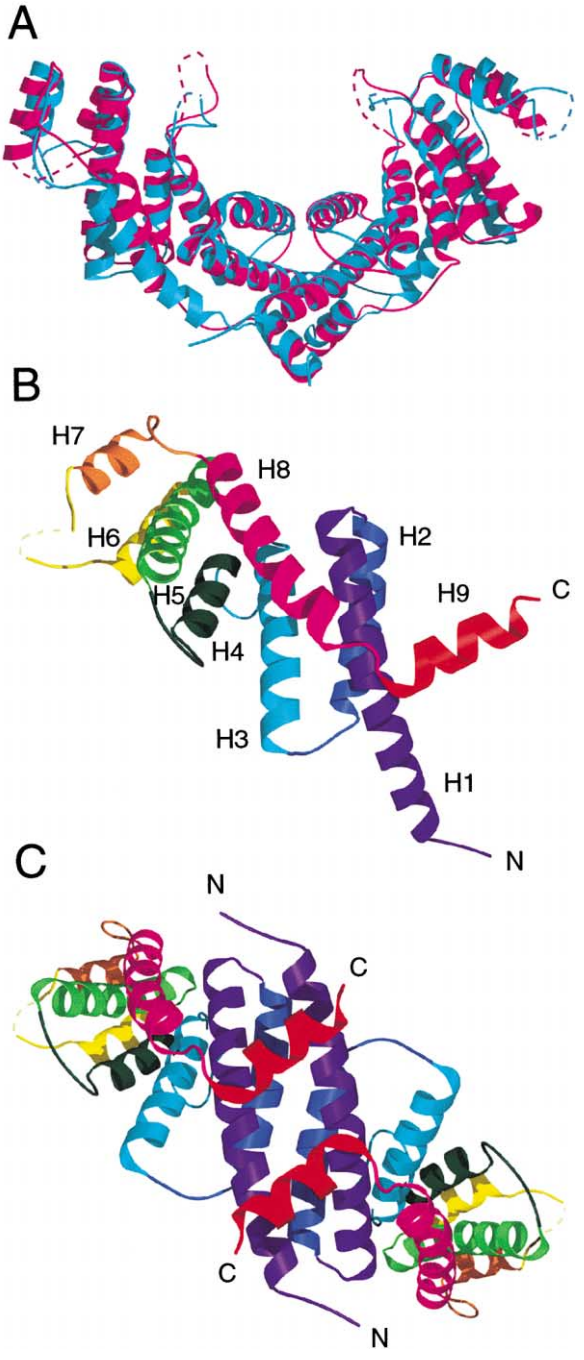

Figure 2. Structure of the Dimerization Domains of TRF1 and TRF2
The structures are shown as ribbon representations. Dotted lines represent regions of structural disorder.

(A) Superposition of the dimerization domains of TRF1 and TRF2 showing the horseshoe shape of the structure. TRF1 is shown in cyan, and TRF2 is shown in magenta.

(B) Structure of a TRFH monomer in the dimerization domain of TRF1. α helices are colored purple to red going from the N to C terminus and are numbered.

(C) View of the dimerization domain of TRF1. The crossbrace formed by helix 9 is also evident in this view. Helices are colored as in (B). The orientation is perpendicular to the view in (A).

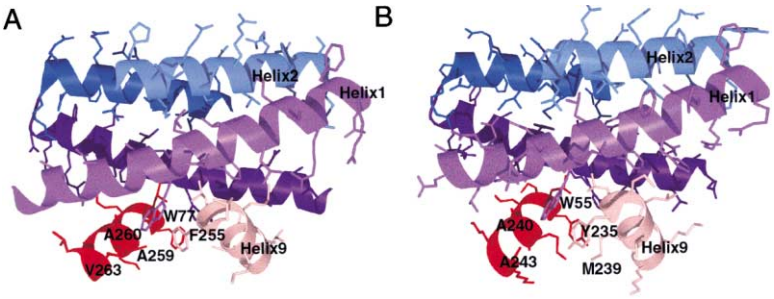

Figure 3. TRF1 and TRF2 Dimer Interfaces Formed by Helices 1, 2, and 9 from Each Monomer

The structures are shown as ribbon representations with amino acid side chains. This view illustrates the multitude of interactions between the helices forming the dimer interface.
(A) TRF1. α helices are colored as in Figure 2B, and one monomer is shown paler than the other for clarity.
(B) TRF2. α helices are colored as in Figure 2B, and one monomer is shown paler than the other for clarity.

TRF1 and TRF2 are very similar, there are some differences in detail (Figure 1B). The most pronounced difference is between the length of helix 8 and its packing against helix 3. In the TRF1 domain it is longer and bent and packs at an angle to helix 3, whereas in TRF2 it packs essentially parallel, resulting in a longer loop between the C terminus of helix 8 and the N terminus of helix 9. A comparison between sequence conservation and amino acid residues used in helix packing interactions shows that the sequence conservation is largely (70%–80%) due to a conservation in the residues involved in forming the structural core (not shown, but see Figure 6).

The Dimer Interface: Why TRF1 and TRF2 Do Not Heterodimerize

The dimer interface, consisting of six α helices (helix 1, 2, and 9 from each monomer), is the part of the structure of the two TRF dimers that is most similar (Figures 2A and 3) with an rmsd for the Cα atoms of 0.88 Å. At the interface, helix 1 from one monomer packs against helix 1 from the other monomer, and, similarly, helix 2 packs with helix 2 forming a symmetrical antiparallel, four-helix bundle. The four-helix bundle is stabilized by the two helix 9 packing against each other and perpendicularly to the two helix 1, forming a crossbrace at the top and the bottom of the dimer interface (Figure 2C).

The interface of each of the two dimers is large, with a buried surface area of 2000 Å^2 for TRF1 and 2247 Å^2 for TRF2. The amino acid side chains involved in forming the dimer interface are highlighted in Figure 1B. The helix 1 to helix 1 packing, which forms the core of the dimer interface, involves a large number of hydrophobic interactions as well as a few hydrogen bonds. Central to the hydrophobic core is the invariant Trp (Trp77 TRF1, Trp55 TRF2) (Figure 4). Trp77 in TRF1 packs against Phe255 (helix 9) within the monomer and between Ala259 and Ala260 and against Val263 of helix 9 from its partner. Similarly, Trp55 in TRF2 packs between Val52 (helix 1) and Tyr235 (helix 9) within the monomer and with Met239 and between Ala240 and Ala243 of helix 9 from its partner (Figures 1B and 3). In TRF1, hydrogen bonds are made across the dimer interface between Glu71 in one monomer with Ser85 in the other monomer. In TRF2 hydrogen bonds across the dimer interface involve residues from both helices 1 and 2: Asn53 to Tyr60, Asp75 to Arg89, and Gln78 to Arg89 (Figures 1B, 4A, and 4C). Helices 1 and 9 are also held together by an extensive hydrophobic core (Figures 2C and 3). The large, hydrophobic, and closely packed nature of the dimer interface explains why TRF1 and TRF2 exist only as dimers and not as monomers. Furthermore, the dimeric structure is a more stable entity than a monomeric TRFH domain would be.

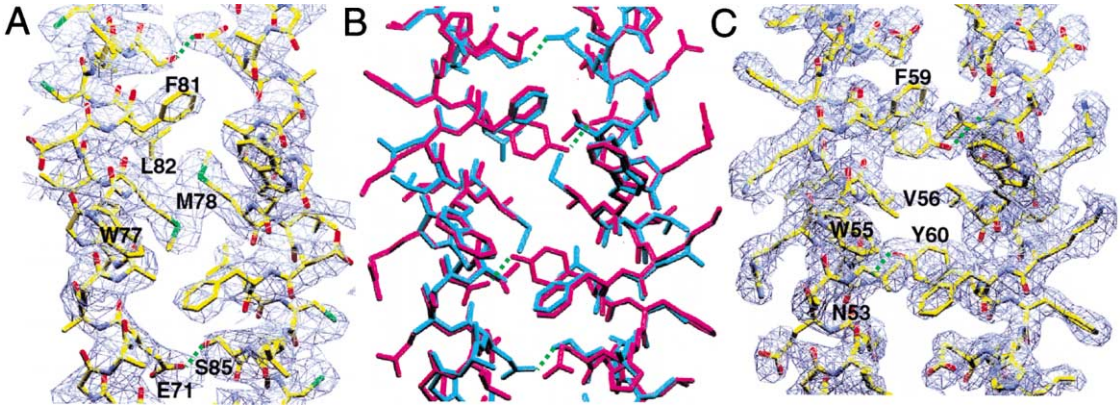

Figure 4. Close-Up Views of the Center of the Dimer Interface Where the Two Helix 1 Cross

The models are shown in their experimental electron density maps after density modification, contoured at 1σ. In each case, the two monomers in the dimer are related in the crystal by a crystallographic dyad axis. The views are down the dyad axis. Green dotted lines indicate hydrogen bonds.
(A) TRF1 dimer interface.
(B) Superposition of TRF1 with TRF2. TRF1 is shown in cyan, and TRF2 is shown in magenta.
(C) TRF2 dimer interface.

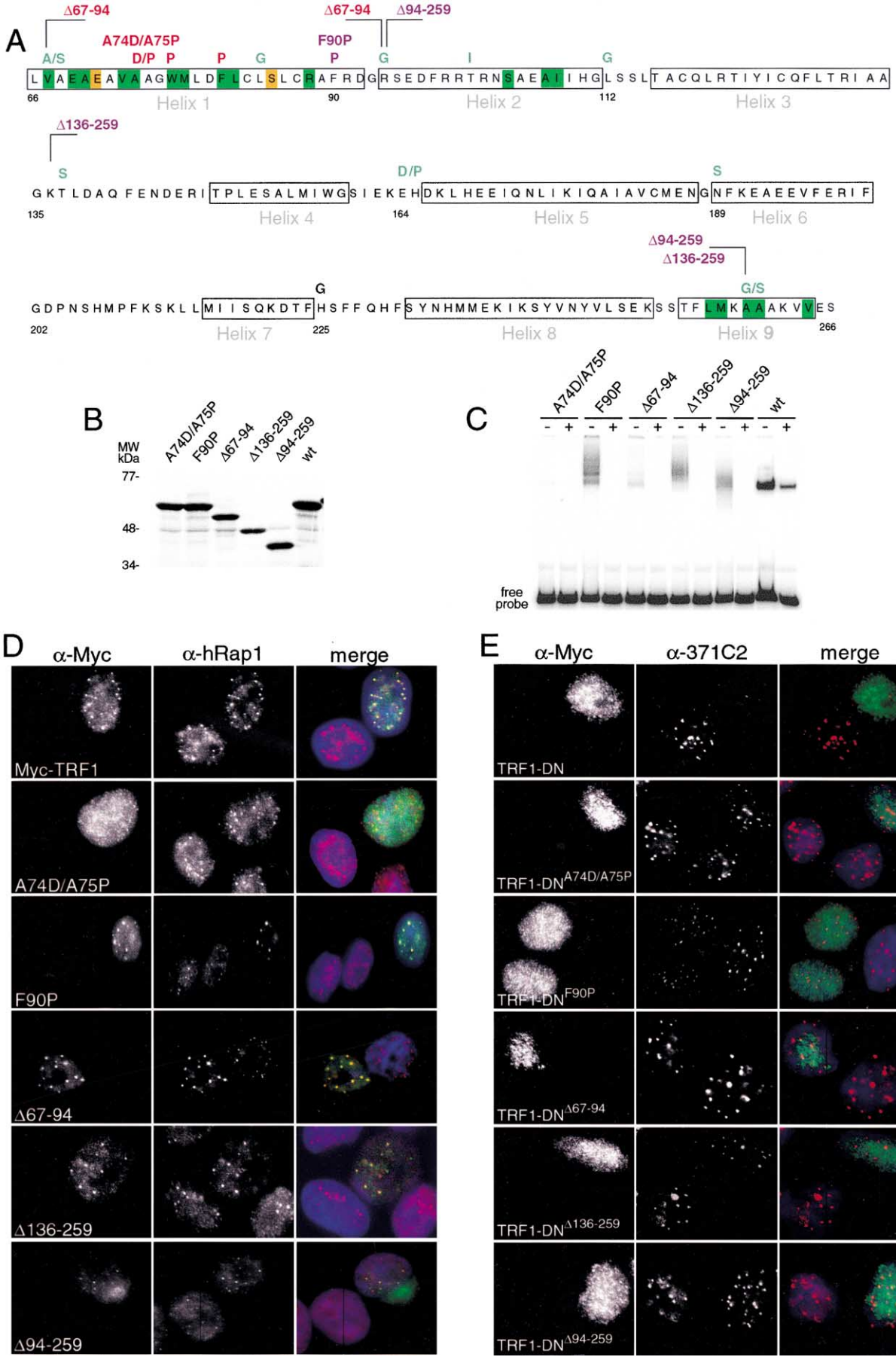

Figure 5. Mutational Analysis of the TRFH Domain of TRF1

A detailed comparison of the 3D structures of the two dimerization domains provides an explanation as to why TRF1 and TRF2 do not heterodimerize with each other. Although their architectures are very similar and a number of interactions are conserved, differences in both the length of the interacting helices and the identity of interacting side chains, as well as different hydrogen-bonding patterns (see above) (Figure 1B), give rise to interfaces that are noncomplementary in both shape and charge (Figure 3). A key difference occurs at the center of the dimer interface where the two helix 1 cross (Figure 4). A superposition of the two interfaces (Figure 4B) shows that Met78 present in TRF1 (Val56 in TRF2), and whose side chain cannot be rearranged, would make a steric clash with Tyr60 present in TRF2 (Leu82 in TRF1), thus preventing heterodimerization (Figure 4B).

A Dimerization Domain Designed for Protein-Protein Interactions

3D structure alignments of the dimerization domain of TRF1 and TRF2 against the structural database using DALI (Holm and Sander, 1993) reveal no common topology. However, the all-helical structure of the two dimers can be viewed as consisting of two parts: a dimer interface formed by α helices 1, 2, and 9 and the arms of the horseshoe formed by α helices 3–8. As might be expected from a protein domain consisting of pairs of α helices, structural alignments of the two parts of the structure reveal features related to other helical proteins. The mode of dimerization by TRF1 and TRF2 is used by many other proteins and is most similar to that of the ColE1 protein Rop, which also forms an antiparallel, four-helix bundle but lacks the crossbrace formed by helix 9 (Banner et al., 1986). The domain forming the arms of the horseshoe, helices 3–7, is related to several proteins consisting of superhelical structures such as Sec 17 (Rice and Brunger, 1999). Such protein scaffolds are known to function as protein-protein interaction surfaces in diverse cellular processes (Rice and Brunger, 1999). Furthermore, a four-helix bundle dimerization interface can itself provide or extend protein-protein interaction surfaces (Newlon et al., 2001).

The architecture of the dimerization domain of the TRFs gives rise to a large surface for interaction with other proteins. This, coupled with the divergence in sequence between the TRFH domains of the human TRFs, results in protein interaction surfaces that are different, consistent with the findings that the TRFH domains of TRF1 and TRF2 are involved in the recruitment of different partners to the telomeres (Kim et al., 1999; Li et al., 2000; L.C. and D.R., unpublished data). A putative kinase GSK-3 site (SEKSS) (Welsh et al., 1997) present in TRF1 but not in TRF2 is accessible on the surface at the C terminus of helix 8. Interestingly, this is the region in the two structures that differs most between TRF1 and TRF2 (Figures 1B and 2A). In summary, the dimerization domains of TRF1 and TRF2 have a common architecture ideally suited for protein recognition but present different protein interaction surfaces as a consequence of their sequence diversity.

Correlation between Structure and Biochemical and Genetic Data

A series of mutations in the TRFH domain of human TRF1 was studied for its effect on the DNA binding activity, which requires formation of TRF1 homodimers in vitro and in vivo. In electrophoretic mobility shift assays with a duplex $(TTAGGG)_{12}$ probe, TRF1 forms a single predominant complex that was previously shown to contain one TRF1 dimer (Bianchi et al., 1997). Of 14 point mutations positioned between residues 66 and 263, three affected the DNA binding activity in multiple independent experiments (mutants A74D/A75P, W77P, and F81P) (Figures 5A–5C). These inhibitory mutations directly affect the dimer interface, and the introduction of a proline residue is likely to alter the structure of this region, corroborating the importance of helix 1 in dimerization. As expected, deletion Δ67–94, which removes helix 1 completely, strongly diminished the DNA binding activity of TRF1, although a minor complex that did not enter the gel was sometimes observed. The contribution of helix 1 to dimerization is further underscored by the deletion mutants Δ94–259 and Δ136–259, which retain helix 1 but lack most of the TRFH domain. Both deletion mutants formed complexes with DNA, but their slower mobility suggests an altered conformation or formation of larger oligomers (Figure 5C). Robust DNA binding activity in combination with slower mobility of the complex was also noted for an additional set of mutants that affect smaller regions of the TRFH domain between positions 90 and 259 (F90P, Δ94–112, Δ112–136, Δ136–188, Δ225–259) (Figures 5A, 5C, and data not shown).

A subset of the TRFH mutants was tested further for telomere binding by transfecting Myc-tagged versions into HeLa cells (Figure 5D). In this setting, wild-type (wt)

(A) Summary of mutations and their phenotypes. Deletion mutations are named after the amino acids flanking the deleted region. Color coding: red, mutations that disrupt dimerization and DNA binding; green, mutations with no effect; purple, mutations resulting in an altered gel-shift complex. Helices 1–9 are boxed, and the dimer interface is color coded as in Figure 1.

(B) SDS-PAGE of in vitro translated ^{35}S-Met-labeled wt and mutant proteins (alleles indicated above the lanes).

C) TTAGGG repeat binding assays using IVT wt and mutant TRF1. Gel-shifts with a ds$[TTAGGG]_{12}$ probe in the presence (+) or absence (−) of unlabeled ds$[TTAGGG]_{27}$ competitor.

(D) Localization of wt and mutant TRF1 alleles to HeLa cell telomeres. IF of transfected myc-tagged wt and mutant TRF1 alleles (as indicated) detected with the Myc antibody (left panels; FITC) in conjunction with an antibody to hRap1 (#666) (Li et al., 2000) (middle panels; TRITC). Merged images are shown in the right panels.

(E) Dominant negative effects of wt and mutant TRF1 alleles. TRFH domain mutations were engineered into a myc-tagged dominant negative allele of TRF1 (TRF1-DN) carrying an inactivating point mutation in the Myb domain (R425V), lacking the acidic N-terminal domain. Left panels: detection of transiently expressed TRF1-DN alleles with a wt or mutant TRFH domain (myc antibody, FITC). Middle panels: same cells probed with antibody 371C2 to the N terminus of TRF1 (TRITC) (van Steensel and de Lange, 1997) absent from TRF1-DN. Right panels: merged images. In (D) and (E), DNA is stained with DAPI.

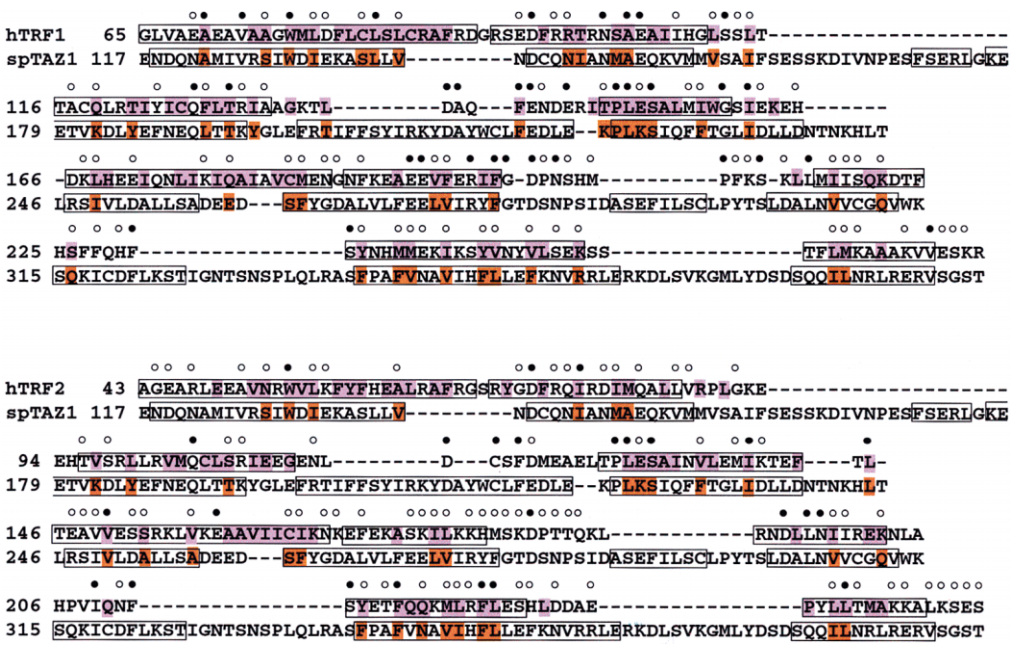

Figure 6. Pairwise Alignments of the TRFH Domain of the Fission Yeast Taz1 with Those of the Human TRF1 and TRF2

Identical residues are indicated by black dots and similar residues by circles. α helices are indicated by boxes. The positions of α helices in TRF1 and TRF2 were taken from the structures (Figure 1), and the positions of α helices in Taz1 were predicted using the program PHD (Rost and Sanders, 1994). The most-buried residues in the two known structures are indicated by lilac shading, and those in the corresponding positions in the aligned Taz1 that are identical or have similar function, according to the Benner-Gonnet matrix (Benner and Gonnet, 1994), are indicated by orange shading.

TRF1 showed the expected localization to telomeres as revealed by colocalization of the punctate-staining pattern of the Myc epitope with the telomeric protein hRap1. By contrast, the helix 1 mutant TRF1$^{A74D/A75P}$ is distributed throughout the nucleoplasm with no obvious accumulation at telomeres. Consistent with the in vitro DNA binding data, TRF1^{F90P}, TRF1$^{\Delta 94–259}$, and TRF1$^{\Delta 136–259}$ localize to telomeres, albeit to a lesser extent than the wt protein. However, unexpectedly, TRF1$^{\Delta 67–94}$ retains the ability to accumulate at telomeres, despite it lacking strong DNA binding activity in vitro. One possibility is that this mutant can form a multimeric complex by tethering to the endogenous TRF1 via other telomeric proteins (e.g., TIN2) (Kim et al., 1999), compensating for its diminished intrinsic dimerization activity.

An alternative explanation for the unexpected ability of TRF1$^{\Delta 67–94}$ helix 1 mutant to accumulate at telomeres could be that the protein heterodimerizes directly with the endogenous TRF1 protein. To test the ability of the mutant alleles to interact with wt TRF1, each of the mutations was engineered into the context of a new dominant negative allele of TRF1, called TRF1-DN here. This protein has a mutation at position 425 (R > V) in the Myb domain that destroys its ability to bind to DNA in vitro and in vivo (Figure 5E and data not shown). TRF1-DN also lacks the N-terminal epitope to the antibody 371C2 (van Steensel and de Lange, 1997), allowing specific detection of the endogenous TRF1 with 371C2 in cells that express TRF1-DN. Using 371C2 to monitor the accumulation of the endogenous TRF1 on telomeres, TRF1-DN can be shown to act as a dominant negative allele, interfering with the telomeric localization of the wt protein in >80% of the transfected nuclei (Figure 5E). Generation of a doubly mutated allele by introduction of the A74D/A75P mutation into TRF1-DN completely destroys this dominant negative effect, consistent with the loss of homodimerization of this mutant (Figure 5E). However, whereas mutation F90P and deletions of 67–94, 94–259, and 94–136 are compatible with homodimerization, these mutations abrogate the ability of TRF1-DN to act as a dominant negative allele (>80% of nuclei showing normal levels of endogenous TRF1 on telomeres). The data suggest that these mutants do not compete effectively with the wt TRF1 for homodimerization. In this regard, the mutants mimic the difference between the dimerization domains of TRF1 and TRF2, which similarly favor homodimerization rather than heterodimerization.

A Possible Structural Similarity between the TRFH Domains of Yeast Taz1 and Human TRFs

We carried out a secondary structure prediction analysis on the TRFH domain of the fission yeast telomeric protein Taz1 using the program PHD (Rost and Sanders, 1994), which accurately predicts the positions of the α helices in both the human TRF1 and TRF2 dimerization domains (not shown). This analysis predicts that the Taz1 TRFH domain also has an all α-helical structure, but because it is larger (about 270 versus the 200 aa of the human TRFs) (Li et al., 2000), it contains additional α-helical elements to the nine helices present in TRF1 and TRF2. The predicted α-helical elements in Taz1 were aligned with those present in TRF1 and TRF2 (Figure 6), and these alignments were used to determine whether

the residues that are buried in the structural core of the TRFH domain of TRF1 and TRF2 (highlighted in Figure 6) and play important roles in helix-helix packing are also present at the appropriate positions within the aligned helices of Taz1. According to this analysis, Taz1 has identical residues or residues that can perform a similar function in about 60% of the buried positions in TRF1 or TRF2 (Figure 6). If the calculation is instead based on comparing Taz1 to both TRF1 and TRF2, the similarity increases to about 75%. This correlation must arise partly from the geometry of helix-helix packing but also from the chemical nature of the side chains at the buried positions. This comparison provides further evidence for the similarity between the TRFH domain of the fission yeast Taz1 and TRF1 and TRF2. However, because of low sequence identity between this family of proteins as well as the low number of known family members, a definitive answer to their structural similarity will have to await the determination of the 3D structure of Taz1.

Conclusions

The dimerization domain of the vertebrate double-strand DNA binding telomeric factors TRF1 and TRF2 is essential for high-affinity DNA binding (Bianchi et al., 1997) and localization to telomeres (van Steensel and de Lange, 1997; van Steensel et al., 1998). It also provides protein interaction surfaces for recruiting other telomeric partners in the formation of the protective telomeric complex. The crystal structures of the conserved TRFH domains of TRF1 and TRF2 reveal a common all α-helical architecture, despite the divergence of their sequences. The specific interactions seen at the dimer interface provide a direct insight into the residues that are important for dimerization. The structural information is corroborated by a mutational analysis of TRF1 that underscores the importance of a functional dimerization interface for DNA binding and telomeric localization.

In addition to permitting only homotypic interactions, the extensive dimer interface imparts stability to the structure and ensures the presence of two Myb binding motifs within one DNA binding unit. The twisted horseshoe shape of the dimerization domain provides a large surface area for interactions with other factors. Because the modest sequence conservation between the human TRFs is due primarily to a conservation of the structural core, it would appear that the TRFH domains evolved to have different surfaces to interact with different telomeric partners, leading to their diverse functions at telomeres. In contrast, the Myb motifs are much more conserved in their sequence, consistent with their common role in recognizing the same telomeric DNA sequence. Furthermore, the structural information on the human TRFs reinforces the proposed evolutionary relationship between vertebrate and fungi telomeric proteins (Li et al., 2000) and suggests that the fission yeast Taz1 TRFH domain has an all-helical structure related to that of the human TRFs.

Experimental Procedures

Protein Expression and Purification

The two constructs encompassing the TRFH domain of hTRF1 and hTRF2, residues 48–268 and residues 42–245, respectively, were expressed in *E. coli* and affinity purified using similar protocols. PCR products were cloned into the pET30a vector (Novagen) modified to contain a Tabacco Etch Virus (TEV) protease cleavage site followed by an N-terminal His6 tag and an S tag. Proteins were produced in the host strain BL21 (DE3). Cell pellets were resuspended in lysis buffer (50 mM Tris/HCl [pH 8.0], 500 mM KCl, 1% Triton X-100, 10 mM mercaptoethanol, 0.5 mM PMSF, and 1 mM benzamidine) and cells disrupted by sonication. After centrifugation (30,000 $\times$ g for 20 min), the supernatant was incubated with Ni-NTA resin (Qiagen) equilibrated in lysis buffer for 30 min. After centrifugation at 1500 rpm, the Ni-NTA resin was washed in wash buffer (50 mM Tris/HCl [pH 8.0], 500 mM KCl, 20 mM imidazole, 10% glycerol, 10 mM mercaptoethanol, 0.5 mM PMSF, and 1 mM benzamidine), and the protein was eluted with wash buffer containing 300 mM imidazole and dialyzed into dialysis buffer (50 mM Tris/Cl [pH 8], 500 mM KCl, 10% glycerol, 10 mM mercaptoethanol, and 0.5 mM PMSF). TEV proteolytic digestions were then performed overnight at room temperature by the addition of TEV protease at a ratio of 1:100 to protein sample. The TEV protease used was itself His_6-tagged. The cleaved proteins were purified away from the TEV protease and the cleaved His tag by repeating the binding to 3 ml of Ni-NTA resin equilibrated in the dialysis buffer. The proteins were then further purified by gel filtration on a Superdex 200 column 26/60 (Pharmacia) also equilibrated in the dialysis buffer. Yields from 3 l cultures were 11 mg and 100 mg for TRF1 and TRF2, respectively. To aid the determination of the structure of the dimerization domain of hTRF2, this protein was produced containing seleno-methionine (Se-Met) as described (Ramakrishnan and Biou, 1996).

Crystallographic Analysis

For both TRF1 and TRF2 dimerization domains, crystals were grown by the hanging drop vapor diffusion method. Drops of 2 or 4 μl were used and contained an equal volume of protein and well solution. Crystallization of the two proteins required different conditions. After purification, TRF1 was dialyzed against 10 mM Tris/HCl (pH 9.0), 200 mM KCl, 10% glycerol, 0.5 mM PMSF, and 10 mM mercaptoethanol and concentrated to 34 mg/ml. Crystals were grown against a well solution containing 100 mM sodium cacodylate (pH 6.0), 5%–15% glycerol, 1–5 mM $Mg(OAc)_2$, and 1% PEG 8000. Crystals were observed within 20 min and grew overnight to a size of 400 μm^3. After purification, TRF2 was first diluted to a final buffer concentration of 20 mM Tris/HCl (pH 8.0), 200 mM KCl, 4% glycerol, 0.4 mM PMSF, 4 mM mercaptoethanol, and subsequently concentrated to 20 mg/ml. Crystals were grown against a well solution containing 100 mM Tris/HCl (pH 7.0), 15%–20% PEG 8000, and 100–200 mM $Mg(OAc)_2$. Crystals were observed within 2 hr and took 1–5 days to reach maximum size.

For data collection, crystals of the TRF1 dimerization domain were frozen at 100K using as cryoprotectant 100 mM sodium cacodylate (pH 6), 30% glycerol, and 5 mM $Mg(OAc)_2$. Crystals were in the spacegroup $P3_12_1$ with unit cell parameters a = 85.39 Å, b = 85.39 Å, c = 91.63 Å, $\alpha = 90^\circ$, $\beta = 90^\circ$, and $\gamma = 120^\circ$. Crystals of TRF2 dimerization domain were frozen using as cryoprotectant 100 mM Tris/HCl (pH 7.0), 18% PEG 8000, 150 mM magnesium acetate, and 20% glycerol. The crystals used for structure determination were C2 with unit cell parameters a = 117.04 Å, b = 80.28 Å, c = 52.82 Å, $\alpha = 90^\circ$, $\beta = 101.95^\circ$, and $\gamma = 90^\circ$. Heavy atom derivatives were obtained for both proteins by soaking methods. For the TRFH domain of TRF2, a seleno-methionine-containing protein was produced, but data from a single wavelength were used (Table 1). The data were collected at SRS Daresbury Laboratory (stations 9.5 and 9.6) and Elettra, Trieste.

The crystallographic statistics for the two structures are shown in Table 1. The data were processed and scaled using MOSFLM (Leslie, 1992) and the CCP4 suite of programs (CCP4, 1994). For both hTRF1 and hTRF2, the heavy atom positions were found using Solve (Terwilliger and Berendzen, 1996) and refined using Sharp (La Fortelle et al., 1997). Solvent flattening was performed using Solomon (Abrahams and Leslie, 1996) implemented within Sharp. The models were built into the electron density using O (Jones et al., 1991). It was immediately apparent that the dimerization domains of both TRF1 and TRF2 were mostly α helical, and initial models were built using polyalanine α helices. The sequence of the first

three helices was easily identified in the TRF1(48–268) map using a mercury position and Trp77 as markers. The amino acid sequence of the rest of TRF1 was identified by superposition with the TRF2 model (42–245), whose sequence was identified using the Se-Met positions. Because there are seven methionines in the sequence apart from the N terminus, the Se-Met sites provided valuable landmarks throughout the TRF2 protein. The asymmetric unit for the TRFH domain of TRF1 contains one monomer, whereas that for TRF2 contains two monomers. For both TRF1 and TRF2, the dimer lies on the crystallographic dyad axis. Model refinement was performed in CNS (Brunger et al., 1998) using noncrystallographic symmetry at the initial stages for TRF2, because it contains two molecules in the asymmetric unit. The model for the dimerization domain of TRF1 (48–268) contains residues 62–265, and that of TRF2 (42–245) contains residues 43–245, with short stretches of the loops between helices 3 and 4 and helices 6 and 7 missing from the electron density maps (residues 139–140 and 205–211 in TRF1 and residues 116–118 and 183–191 in TRF2). Illustrations of the structures were prepared using Molscript (Kraulis, 1991), Povscript and Pov-Ray, and Swiss PdbViewer (Guex and Peitsch, 1997).

TRF1 Mutagenesis

Site-directed mutagenesis of the hTRF1 cDNA in pET28a (Bianchi et al., 1997) was performed by PCR using forward and reverse oligonucleotides representing the desired mutations (sequences available on request). PCR products were digested with DpnI and transformed into XL-1 Blue cells, and the resulting mutants were sequenced. Deletion mutants were generated by creating a unique BamHI site at different positions via mutagenesis (as above), cutting with BamHI-EcoRI, and ligating various backbones and inserts to create desired deletions. For transfection experiments, the TRF1 mutants were cloned into the HindII-EcoRI sites of pCDNA3 carrying an N-terminal myc tag (J. Karlseder and T.d.L., unpublished data) via PCR (Pfu polymerase, Stratagene) using 5′-GCGC AAG CTT GCG GAG CAT GTT TCC TCA G-3′ as a forward primer and 5′-GCGC GAA TTC TCA GTC TTC GCT GTC TGA G-3′ as a reverse primer. To create the mutants in the dominant negative allele TRF1-DN, the following strategy was used: a TRF1 construct was generated by two-step site-directed mutagenesis introducing the R425V mutation that destroys the DNA binding activity as well as a silent mutation that introduced a new restriction site at position 310 (310G–311T yields a KpnI site). The KpnI-EcoRI fragment from this construct spanning amino acids 310–439, including R425V, was moved into pCDNA3 with the N-terminal myc tag and used as an acceptor plasmid for introduction of PCR fragments representing amino acids 66–310 from the relevant mutants using 5′-GCGC AAG CTT GTG GCC GAG GCC GAG GCC GTG-3′ as a forward primer and 5′-GCGC GGT ACC CTC TGA GGA TTC AGT TAC-3′ as a reverse primer. The resulting alleles contained aa 66–439 of TRF1 with the R425V mutation in the Myb domain and the various TRFH domain mutations as indicated in the text.

In Vitro Transcription/Translation and DNA Binding Assays

Expression of TRF1 and derivatives were performed as described previously (Bianchi et al., 1997). Plasmid DNA (0.2–0.5 μg per 20 μl reaction) was used in the presence or absence of ^{35}S-Methionine. Labeled products were visualized on a 9% SDS-PAGE gel, and unlabeled products were diluted 1:1 with buffer D (Chong et al., 1995), and 2 μl was used for gel-shift assays. Gel-shift assays were performed as previously described (Bianchi et al., 1997; Zhong et al., 1992) using the ^{32}P-labeled 142 bp HindIII-Asp718 fragment of the plasmid pTH12 (Zhong et al., 1992) as a probe, which contains 12 tandem TTAGGG repeats. Competition experiments were performed with a 100-fold excess of the 200 bp EcoRI fragment of pTH5, which contains 27 tandem TTAGGG repeats (de Lange et al., 1990).

Subnuclear Localization

Subnuclear localization was determined in the HeLa1.2.11 subclone (Griffith et al., 1999), electroporated with either wt or mutant myc-tagged TRF1 alleles (20 μg DNA, 8×10^6 cells in 0.8 ml; 280V/960 μF). Cells were grown for 24 hr on Alcian blue-coated coverslips and processed as described previously (Chong et al., 1995; van Steensel and de Lange, 1997). TRF1 mutants were detected with the anti-myc antibody 9E10 (Austrian Biocenter). RapI was visualized using the anti-Rap1 antibody 666 (Li et al., 2000). In the experiments with TRF1-DN constructs, wt TRF1 was visualized with the antibody 371C2 (van Steensel and de Lange, 1997). Rabbit antibodies were detected with TRITC-conjugated donkey-anti-rabbit antibodies (Jackson Immunoresearch), and mouse antibodies were visualized with FITC-conjugated donkey-anti-mouse antibodies (Jackson Immunoresearch). Experiments in which one of the two primary antibodies was omitted showed that there was no significant bleed-through between the red and green channels. DNA was stained with 4′,6′-diamidino-2-phenylindole. Micrographs were recorded using fixed settings on a Zeiss Axioplan II microscope with a Hammamatsu C4742-95 camera using Open Lab software.

Acknowledgments

We thank John Schwabe, Pietro Roversi, Luca Jovine, and James Love for their help with data collection and processing and map calculations, Alexey Murzin, Loredana Lo Conte, and Veronica Morea for their help with protein structure analyses, and Ian Fearnley for mass spectrometry. We thank the staff at the Daresbury Laboratory and Elettra for help with data collection. This work was supported by a grant from the Human Frontiers Sciences Program to D.R and T.d.L and by grants to T.d.L from the NIH (GM49046 and CA76027).

Received March 29, 2001; revised June 20, 2001.

References

Abrahams, J.P., and Leslie, A.G.W. (1996). Methods used in the structure determination of bovine mitochondial F_1 ATPase. Acta Crystallogr. D *52*, 30–42.

Banner, D.W., Kokkinidis, M., and Tsernoglou, D. (1986). Structure of ColE1 Rop protein at 1.7Å resolution. J. Mol. Biol. *196*, 657–675.

Benner, S.A., and Gonnet, G.H. (1994). Amino acid substitution during functionally constrained divergent evolution of protein sequences. Protein Eng. *7*, 1323–1332.

Bianchi, A., Smith, S., Chong, L., Elias, P., and de Lange, T. (1997). TRF1 is a dimer and bends telomeric DNA. EMBO J. *16*, 1785–1794.

Bianchi, A., Stansel, R.M., Fairall, L., Griffith, J.D., Rhodes, D., and de Lange, T. (1999). TRF1 binds a bipartite telomeric site with extreme spatial flexibility. EMBO J. *18*, 5735–5744.

Broccoli, D., Chong, L., Oelmann, S., Fernald, A.A., Marziliano, N., van Steensel, B., Kipling, D., Le Beau, M.M., and de Lange, T. (1997). Comparison of the human and mouse genes encoding the telomeric protein, TRF1: chromosomal localization, expression and conserved protein domains. Hum. Mol. Genet. *6*, 69–76.

Broccoli, D., Smogorzewska, A., Chong, L., and de Lange, T. (1997). Human telomeres contain two distinct Myb-related proteins, TRF1 and TRF2. Nat. Genet. *17*, 231–235.

Broccoli, D., Godley, L.A., Donehower, L.A., Varmus, H.E., and de Lange, T. (1996). Telomerase activation in mouse mammary tumors: lack of detectable telomere shortening and evidence for regulation of telomerase RNA with cell proliferation. Mol. Cell. Biol. *16*, 3765–3772.

Brunger, A.T., Adams, P.D., Clore, G.M., Delano, W.L., Gros, P., Grosse-Kunstleve, R.W., Jiang, J.-S., Kuszewski, J., Nilges, M., Pannu, N.S., et al. (1998). Crystallography and NMR system: A new software suite for macromolecular structure determination. Acta Crystallogr. D *54*, 905–921.

CCP4 (Collaborative Computational Project 4) (1994). The CCP4 suite: programs for protein crystallography. Acta Crystallogr. D *50*, 760–763.

Chong, L., van Steensel, B., Broccoli, D., Erdjument-Bromage, H., Hanish, J., Tempst, P., and de Lange, T. (1995). A human telomeric protein. Science *270*, 1663–1667.

Cooper, J.P., Nimmo, E.R., Allshire, R.C., and Cech, T.R. (1997). Regulation of telomere length and function by a Myb-domain protein in fission yeast. Nature *385*, 744–747.

de Lange, T., Shiue, L., Myers, R.M., Cox, D.R., Naylor, S.L., Killery,

A.M., and Varmus, H.E. (1990). Structure and variability of human chromosome ends. Mol. Cell. Biol. *10*, 518–527.

Ferreira, M.G., and Cooper, J.P. (2001). The fission yeast Taz1 protein protects chromosomes from Ku-dependent end-to-end fusions. Mol. Cell *7*, 55–63.

Griffith, J., Bianchi, A., and de Lange, T. (1998). TRF1 promotes parallel pairing of telomeric tracts in vitro. J. Mol. Biol. *278*, 79–88.

Griffith, J.D., Comeau, L., Rosenfield, S., Stansel, R.M., Bianchi, A., Moss, H., and de Lange, T. (1999). Mammalian telomeres end in a large duplex loop. Cell *97*, 503–514.

Guex, N., and Peitsch, M.C. (1997). SWISS-MODEL and the Swiss-PdbViewer: an environment for comparative protein modeling. Electrophoresis *18*, 2714–2723.

Holm, L., and Sander, C. (1993). Protein structure comparison by alignment of distance matrices (Dali 2.0). J. Mol. Biol. *233*, 123–138.

Jones, T.A., Zou, J.-Y., Cowan, S.W., and Kjeldgaard, M. (1991). Improved methods for building protein models in electron density maps and the location of errors in these models. Acta Crystallogr. A *47*, 110–119.

Karlseder, J., Broccoli, D., Dai, Y., Hardy, S., and de Lange, T. (1999). p53- and ATM-dependent apoptosis induced by telomeres lacking TRF2. Science *283*, 1321–1325.

Kim, S.H., Kaminker, P., and Campisi, J. (1999). TIN2, a new regulator of telomere length in human cells. Nat. Genet. *23*, 405–412.

Konig, P., and Rhodes, D. (1997). Recognition of telomeric DNA. Trends Biochem. Sci. *22*, 43–47.

Konig, P., Giraldo, R., Chapman, L., and Rhodes, D. (1996). The crystal structure of the DNA-binding domain of yeast RAP1 in complex with telomeric DNA. Cell *85*, 125–136.

Konig, P., Fairall, L., and Rhodes, D. (1998). Sequence-specific DNA recognition by the myb-like domain of the human telomere binding protein TRF1: a model for the protein-DNA complex. Nucleic Acids Res. *26*, 1731–1740.

Kraulis, P.J. (1991). MOLSCRIPT: a program to produce both detailed and schematic plots of protein structures. J. Appl. Crystallogr. *24*, 946–950.

La Fortelle, E., Irwin, J.J., and Bricogne, G. (1997). Advances in MIR and MAD phasing: maximum-likelihood refinement in a graphical environment, with SHARP. In Proceedings of the CCP4 Study Weekend, G.D.K.S. Wilson, A.W. Ashton, and S. Bailey, eds. (Warrington, UK: CCLRC Daresbury Laboratory).

Leslie, A.G.W. (1992). Recent changes to the MOSFLM package for processing film and image plate data. In Joint CCP4 and ESF-EAMCB Newsletter on Protein Crystallography (Warrington, UK: Daresbury Laboratory).

Li, B., Oestreich, S., and de Lange, T. (2000). Identification of human Rap1: implications for telomere evolution. Cell *101*, 471–483.

Lundblad, V. (2000). DNA ends: maintenance of chromosome termini versus repair of double strand breaks. Mutat. Res. *451*, 227–240.

Marcand, S., Wotton, D., Gilson, E., and Shore, D. (1997a). Rap1p and telomere length regulation in yeast. Ciba. Found. Symp. *211*, 76–93.

Marcand, S., Gilson, E., and Shore, D. (1997b). A protein-counting mechanism for telomere length regulation in yeast. Science *275*, 986–990.

McEachern, M.J., Krauskopf, A., and Blackburn, E.H. (2000). Telomeres and their control. Annu. Rev. Genet. *34*, 331–358.

Munoz-Jordan, J.L., Cross, G.A.M., de Lange, T., and Griffith, J.D. (2001). T-loops at trypanosome telomeres. EMBO J. *20*, 579–588.

Murti, K.G., and Prescott, D.M. (1999). Telomeres of polytene chromosomes in a ciliated protozoan terminate in duplex DNA loops. Proc. Natl. Acad. Sci. USA *96*, 14436–14439.

Nakamura, T.M., Cooper, J.P., and Cech, T.R. (1998). Two modes of survival of fission yeast without telomerase. Science *282*, 493–496.

Newlon, M.G., Roy, M., Morikis, D., Carr, D.W., Westphal, R., Scott, J.D., and Jennings, P.A. (2001). A novel mechanism of PXA anchoring by solution structures of anchoring complex. EMBO J. *20*, 1651–1662.

Nimmo, E.R., Pidoux, A.L., Perry, P.E., and Allshire, R.C. (1998). Defective meiosis in telomere-silencing mutants of *Schizosaccharomyces pombe*. Nature *392*, 825–828.

Nishikawa, T., Nagadoi, A., Yoshimura, S., and Nishimura, Y. (1998). Solution structure of the DNA-binding domain of human telomeric protein, hTRF1. Structure *6*, 1057–1065.

Ogata, K., Morikawa, S., Nakamura, H., Sekikawa, A., Inoue, T., Kanai, H., Sarai, A., Ishii, S., and Nishimura, Y. (1994). Solution structure of a specific DNA complex of the Myb DNA-binding domain with cooperative recognition helices. Cell *79*, 639–648.

Ramakrishnan, V., and Biou, V. (1996). Treatment of MAD data as a special case of MIR. Methods Enzymol. *276*, 538–557.

Rice, L.M., and Brunger, A.T. (1999). Crystal structure of the vesical transport protein Sec17: implications for SNAP function in SNARE complex disassembly. Mol. Cell *4*, 85–95.

Rost, B., and Sanders, C. (1994). Combining evolutionary information and neural networks to predict protein secondary structure. Proteins *19*, 55–72.

Smith, S., and de Lange, T. (2000). Tankyrase promotes telomere elongation in human cells. Curr. Biol. *10*, 1299–1302.

Smith, S., Giriat, I., Schmitt, A., and de Lange, T. (1998). Tankyrase, a poly(ADP-ribose) polymerase at human telomeres. Science *282*, 1484–1487.

Smogorzewska, A., van Steensel, B., Bianchi, A., Oelmann, S., Schaefer, M.R., Schnapp, G., and de Lange, T. (2000). Control of human telomere length by TRF1 and TRF2. Mol. Cell. Biol. *20*, 1659–1668.

Spink, K.G., Evans, R.J., and Chambers, A. (2000). Sequence-specific binding of Taz1 dimers to fission yeast telomeric DNA. Nucleic Acids Res. *28*, 527–533.

Terwilliger, T.C., and Berendzen, J. (1996). Correlated phasing of multiple isomorphous replacement data. Acta Crystallogr. D *52*, 749–757.

van Steensel, B., and de Lange, T. (1997). Control of telomere length by the human telomeric protein TRF1. Nature *385*, 740–743.

van Steensel, B., Smogorzewska, A., and de Lange, T. (1998). TRF2 protects human telomeres from end-to-end fusions. Cell *92*, 401–413.

Welsh, G.I., Patel, J.C., and Proud, C.G. (1997). Peptide substrates for assaying glycogen synthase kinase-3 in crude cell extracts. Anal. Biochem. *244*, 16–21.

Zhong, Z., Shiue, L., Kaplan, S., and de Lange, T. (1992). A mammalian factor that binds telomeric TTAGGG repeats in vitro. Mol. Cell. Biol. *12*, 4834–4843.

Zhu, X.D., Kuster, B., Mann, M., Petrini, J.H., and Lange, T. (2000). Cell-cycle-regulated association of RAD50/MRE11/NBS1 with TRF2 and human telomeres. Nat. Genet. *25*, 347–352.

Accession Numbers

Atomic coordinates for both structures have been deposited with the Protein Data Bank hTRF1 TRFH domain under ID Code 1h6o and hTRF2 TRFH domain under ID code 1h6p.